Imaging and Radiation Research (2020) Volume 3 Issue 1
doi:10.24294/irr.v3i1.1723

ORIGINAL RESEARCH ARTICLE

Pulmonary dynamics of anatomical structures of interest in 4DCT imaging

Sarahí Hernández-Juárez, Aldo Rodrigo Mejía-Rodríguez*, Edgar R. Arce-Santana

Facultad de Ciencias, Universidad Autónoma de San Luis Potosí (UASLP), S.L.P., Mexico. E-mail: aldo.mejia@uaslp.mx

ABSTRACT

The present work shows an application of the Chan-Vese algorithm for the semi-automatic segmentation of anatomical structures of interest (lungs and lung tumor) in 4DCT images of the thorax, as well as their three-dimensional reconstruction. The segmentation and reconstruction were performed on 10 CT images, which make up an inspiration-expiration cycle. The maximum displacement was calculated for the case of the lung tumor using the reconstructions of the onset of inspiration, the onset of expiration, and the voxel information. The proposed method achieves appropriate segmentation of the studied structures regardless of their size and shape. The three-dimensional reconstruction allows us to visualize the dynamics of the structures of interest throughout the respiratory cycle. In the future, it is expected to have more evidence of the good performance of the proposed method and to have the feedback of the clinical expert, since the knowledge of the characteristics of anatomical structures, such as their dimension and spatial position, helps in the planning of Radiotherapy (RT) treatments, optimizing the radiation dose to cancer cells and minimizing it in healthy organs. Therefore, the information found in this work may be of interest for the planning of RT treatments.

Keywords: Segmentation; Chan-Vese; Lung Dynamics; 4DCT Chest Images

ARTICLE INFO

Received: 11 February 2020
Accepted: 2 April 2020
Available online: 15 April 2020

1. Introduction

Medical imaging is one of the most powerful tools in the clinical setting due to its ability to show anatomical and functional information of the human body, which can be used for the diagnosis of diseases and the evaluation or follow-up of medical treatments through the analysis of anatomical structures of interest such as bones, healthy structures or structures affected by a tumor (lungs, brain, prostate, etc.), or the tumor itself[1]. For example, in Radiation Therapy (RT), patients undergoing radiation treatment for cancer usually present loss in the volume of the tumor and the surrounding healthy organs (organs at risk), which causes a decrease in the functionality of these organs as a side effect of the therapy. For this reason, knowledge of the characteristics of these structures, such as their size and spatial position, makes it possible to plan the treatment, optimizing the radiation dose to the tumor and minimizing the dose absorbed by healthy organs[2].

One of these treatments is Tomotherapy, which delivers high energy ionizing radiation in a modulated manner, being able to create very strong dose distributions around target volumes (tumors). However, during radiation, patients may undergo significant anatomical changes due to physiological processes, as in the case of the lungs, which can modify their volume and shape considerably due to the movements

caused by breathing (inspiration-expiration cycle)[3].

As a direct consequence, there are discrepancies between the planned dose distribution and the actual dose[4], which increases the importance of analyzing and studying the anatomical changes of the lungs during the respiratory cycle in order to target the corresponding radiation dose and thus improve treatment efficiency.

For the analysis of anatomical structures of interest in RT treatments, one of the most critical and complicated steps is the extraction of these structures by means of a segmentation process. This segmentation process can be performed either manually by a clinical expert (which involves a great deal of time and effort), or by segmentation algorithms. In the literature it is possible to find different image segmentation algorithms based on: intensity (gray levels) of the pixels or voxels of the image, thresholding, spatial features, fuzzy sets, among others[5-7].

These methods seek to obtain a good balance between accuracy, noise robustness and computation time. In particular, the noise factor is of vital importance for medical imaging, since it is always present and can be of different types, depending on the imaging technology used for its acquisition, the pathology present in the patient, internal movements of physiological processes, among other factors, so defining a standard segmentation algorithm for medical imaging remains an open problem.

A quantitative evaluation of the performance of the classical K-means and Otsu segmentation algorithms (methods widely used in clinical settings), and an algorithm based on the Chan-Vese method, is presented by Hernandez *et al.*[8], for the segmentation of anatomical structures of interest with complex shapes (such as lungs and tumors) in medical Computed Axial Tomography (CT); in this work it was shown that the three methods studied have a good performance for the segmentation of large structures (such as lungs), however, the algorithm based on the Chan-Vese method was the most robust and accurate for tumor segmentation (compared to the segmentation performed manually by a clinical expert). For this reason, this paper proposes the use of this active contouring method for the segmentation of the lungs and a lung tumor in 4D CT (4DCT) medical images[9], i.e., a set of volumetric images acquired at specific time periods of the respiratory cycle.

For this reason, the objective of this work is to segment the volume corresponding to the structures of interest of the lungs and a lung tumor in order to obtain information that could be useful for the planning of a RT treatment, related to the dynamics of these structures throughout the respiratory cycle. Additionally, as a complement to 4DCT image segmentation, this work proposes the use of three-dimensional reconstruction and visualization tools to have a clearer representation of the changes that occur during the respiratory cycle.

2. Methodology

The Chan-Vese method has proven to be very useful to achieve the segmentation of various objects or anatomical structures in images with a large amount of noise, or where the edges of the objects of interest are not well defined. There are works in the literature in which the Chan-Vese method is used for the segmentation of anatomical structures such as small intestine and blood vessels, as well as in the industrial field for the extraction of carburetors, tires and other automotive parts[10–12]. In general, the Chan-Vese algorhythm is a segmentation method where the minimization of an energy functional is sought. In this work, the original proposal of the method developed by Chan and Vese[13] is used as a basis, to carry out our implementation by extending the classical method, which works with 2D images, to work with volumetric images and obtain the segmentation of the lungs and the lung tumor in 3D.

2.1 Theoretical Basis—Chan-Vese Algorithm

For the description of the Chan-Vese method, it can be assumed that an image I consists of two regions of different homogeneous intensities, in this case I^i and I^o, where the object to be detected is represented by the region I, i.e. the area that belongs to the object, which is delimited by a curve C; while I^o is the area that does not belong to the object. The

energy functional can be defined taking into consideration the region I^i, as the area inside the curve (Cin) and I^o as the region outside the curve (Cout), as follows:

$$F_1(C) + F_2(C) = \int_{Cin} |I - C_1|^2 dxdy + \int_{Cout} |I - C_2|^2 dxdy \quad (1)$$

where C is a variable curve and the constants C_1 and C_2 correspond to the average value of the intensity of the image pixels I inside and outside the C curve. When the curve C is outside the area of interest, we have that $F_1(C) > 0$ and $F_2(C) \approx 0$, while if $F_1(C) \approx 0$ and $F_2(C) > 0$ are the cases, the curve is inside the area. It is said that the minimization of the energy functional occurs when the curvature is outlining the contour of the object to be segmented, i.e., when $F_1(C) \approx 0$ and $F_2(C) \approx 0$. To this model we add some regularization terms such as the length of the curve C, and the area inside C, defining now the energy functional shown below:

$$\begin{aligned} F(C_1, C_2, C) = \mu \cdot Longitud(C) + v \cdot Area(adentro(C)) \\ + \lambda_1 \int_{Cin} |I - C_1|^2 dxdy \\ + \lambda_2 \int_{Cout} |I - C_2|^2 dxdy, \end{aligned} \quad (2)$$

where $\mu \geq 0$, $v \geq 0$ are constant regularization parameters and $\lambda_1, \lambda_2 > 0$ are constant weight parameters dependent on the image I. Under this principle, the curve C is represented by a zero-level curve of a Lipschitz function (φ) using level sets, the energy function remaining in terms of φ. On the other hand, the signs taken by this function can be represented by means of the Heaviside function, $H(\Phi)$:

$$H(\phi) = \begin{cases} 1 & \text{si } \phi > 0 \\ 0 & \text{si } \phi < 0 \end{cases} \quad (3)$$

The derivative of $H(\Phi)$ is the Dirac delta function (δ_0), which can be approximated by:

$$\delta_0 = \frac{\epsilon}{\pi(\epsilon^2 + \phi^2)} \quad (4)$$

i.e., δ_0 is the approximation to the Dirac delta function when ε tends to zero. Based on the above, the energy function can be written as:

$$\begin{aligned} F(C_1, C_2, \phi) = \mu \int \delta_0 | \bigtriangledown \phi | dxdy \\ + v \int H(\phi) dxdy + \lambda_1 \int |I - C_1|^2 H(\phi) dxdy \\ + \lambda_2 \int |I - C_2|^2 (1 - H(\phi)) dxdy \end{aligned} \quad (5)$$

Keeping fixed and minimizing the energy of $F(C_1, C_2, \Phi)$ with respect to the constants C_1 and C_2, these can be written in terms of:

$$\begin{aligned} C_1(\phi) = \frac{\int I \cdot H(\phi) dxdy}{\int H(\phi) dxdy} \\ C_2(\phi) = \frac{\int I \cdot (1 - H(\phi)) dxdy}{\int (1 - H(\phi)) dxdy} \end{aligned} \quad (6)$$

On the other hand, in order to minimize the functional (5) in terms of the function Φ, its first variation is defined by means of the Euler-Lagrange equation. Using these considerations, the difference equation can be written as follows:

$$\begin{aligned} \frac{dF}{d\phi} = \bigtriangledown F = \delta_0(\phi) \left[-\mu \cdot \bigtriangledown \left(\frac{\bigtriangledown \phi}{| \bigtriangledown \phi |} \right) \right. \\ \left. + v + \lambda_1 (I - C_1)^2 - \lambda_2 (I - C_2)^2 \right] \end{aligned} \quad (7)$$

For the practical part and implementation of the algorithm, the discrete version of equation (7) is used, thus achieving the delimitation of the object to be segmented through the evolution of the curve. Using the gradient de-census, an artificial variable is introduced with respect to time as follows:

$$\frac{d\phi}{dt} = - \bigtriangledown F = \frac{\phi^{t+1} - \phi^t}{\Delta t} \quad (8)$$

In this version of the Chan-Vese method, the number of iterations (n) and the time between each iteration (Δt) must be taken into account. The discrete form of the minimization of the energy functional is shown below:

$$\phi^{n+1} = \phi^n - \bigtriangledown F \cdot \Delta t \quad (9)$$

2.2 Implementation of the Chan-Vese Segmentation Algorithm in 3D

In this work, modifications were made to the model described in the previous section in order to perform the segmentations of the structures of interest volumetrically. That is, the energy functions described above were modified to work along the three cartesian axes (x, y, z), i.e., the functions are generalized to work in the entire imaging domain. The energy function of the model is described as follows:

$$\begin{aligned} F(C_1, C_2, S) = \mu \cdot Area(S) + v \cdot Volumen(adentro(S)) \\ + \lambda_1 \int_{Sin} |I - C_1|^2 d\Omega + \lambda_2 \int_{Sout} |I - C_2|^2 d\Omega \end{aligned} \quad (10)$$

where S is the variable surface, *Sin* is the domain of the internal region of the object, *Sout* the external region and Ω represents the image domain. The first part of the function refers to the regularization terms considered, in this case the surface area and

the interim volume of the surface, which were suitable for working with the domain of the energy function.

The other terms describe the expansion movement of the surface when it is inside the area or object; and the contraction movement when it is outside the object. With Φ being the zero level representing the active contour, the functional proposed to be minimized is as follows:

$$F(C_1, C_2, \phi) = \mu \int_\Omega \delta(\phi)| \bigtriangledown \phi| d\Omega + v \int_\Omega H(\phi) d\Omega + \lambda_1 \int_\Omega |I - C_1|^2 H(\phi) d\Omega + \lambda_2 \int_\Omega |I - C_2|^2 (1 - H(\phi)) d\Omega \quad (11)$$

Once the above functional is derived with respect to the Φ term (to achieve its minimization) by means of the Euler-Lagrange equation, the resulting difference equation can be written in the same way as equation (7). In order to achieve the delimitation of the object of interest through the evolution of the surface, the discrete version of the difference equation is also used considering the number of iterations and the time between each iteration, as shown in equation (9). To facilitate the implementation of the proposed algorithm described above, in equation (7) it was considered that $\delta_0(\Phi) = 1$ and $v = 0$ based on tests performed by Chan and Vese[13], in addition to an update in order to calculate the sign of the zero-level set of the function, resulting in the following expression:

$$\phi^{n+1} = \phi^n + \Delta t \left[\mu \cdot \bigtriangledown \left(\frac{\bigtriangledown \phi}{| \bigtriangledown \phi|} \right) - \lambda_1 (I - C_1)^2 + \lambda_2 (I - C_2)^2 \right] \quad (12)$$

The values of the λ_1 and λ_2 terms in the above expression were calculated from the intensities of the voxels inside and outside the curve. To achieve this objective, the thresholds of the lungs and the lung tumor were calculated from the information of the original image using the Otsu method[7], implemented in MatLab® by means of the multi-thresh function, which returns the threshold that allows us to differentiate the objects or areas of interest, in this case the lungs or the tumor, with respect to the background. Once the thresholds were determined, we obtained the variances of those values of the image that would exceed these thresholds (background), as well as the opposite case, where the values correspond to one of the desired anatomical structures. Thus, the values of *λ's* are obtained by calculating the inverse of the variances obtained.

Additionally, as initial curve in both cases the whole set of masks resulting from a previous segmentation of the images with the K-means method was used, which is a method based on the grouping of clusters represented with a weighted average of pixels called centroids. The main foundation of the algorithm is to define K centroids (one for each group of data of interest) within the image to be processed[6]. For this initialization, the MatLab® *kmeans* function was used, in which the number of clusters to be obtained must be specified. In this case, 2 clusters were defined, which made it possible to differentiate the anatomical structure of interest (lungs or lung tumor) from the other information in the image (background and other structures).

For all segmentations performed, the parameters μ and Δt had a value of 0.1. In the lung segmentation, the constants C_1 and C_2 were calculated with the average of the pixels of the entire volume taking into account when $\Phi \geq 0$ and $\Phi < 0$ respectively; while in the case of the tumor segmentation, the calculation of the constants was carried out with the help of a subvolume, where it was only possible to delimit the pixels of the object, thus facilitating the location of the area where the structure was located.

Finally, the number of iterations used for lung and tumor segmentation were set to 10 and 5 respectively. These values were defined by means of a segmentation consistency test, where the minimum number of iterations necessary to obtain a segmentation that differed by less than 1% with respect to a segmentation generated with a maximum number of 100 iterations was sought.

Given the characteristics of the proposed method, in each iteration of the algorithm the entire volume of the images is used, which means that the operations of the discrete function of the algorithm are performed in a three-dimensional way, thus ob-

taining the evolution of a surface. In summary, the evolution of the implemented segmentation algorithm can be approached using the following strategy (**Figure 1**):

1. Initializer ϕ^n with initial mask.
2. Calculate C_1 & C_2.
3. Solve the equation: $\phi^{n+1} = \phi^n + \Delta t\,[-\lambda_1(I - C_1)^2 + \lambda_2(I - C_2)^2]$.
4. Actualize ϕ^{n+1}, in order to achieve zero level curve sign adjustment.
5. Solve the missing term in equation (12): $\nabla\left(\frac{\nabla\phi}{|\nabla\phi|}\right)$.
6. Perform the above steps until you get a stationary ϕ value.

Figure 1. Strategy for the evolution of the implemented algorithm.

2.3 4DCT chest images

For the analysis of the Chan-Vese algorithm, a set of 4DCT chest images obtained from the database of the Léon Bérard Cancer Center and the Biomedical Imaging Research Laboratory (CREATIS lab) in Lyon, France[9] was selected, where it is possible to observe pulmonary structures together with their internal characteristics (bronchial ramifications) and a large pulmonary tumor located in the right lung. This 4D dataset is made up of 10 CT images that were acquired from a patient in different phases of the respiratory cycle, i.e., one inspiration-expiration cycle is divided into 10 CT images. Each of the CT images has a size of 475 × 335 × 123 voxels, with a voxel dimension of 0.98 mm × 0.98 mm × 2.00 mm.

2.4 Quantitative analysis of the performance of the segmentation method

To validate the accuracy of the volumetric segmentations obtained with the implemented algorithm based on the Chan-Vese method, the differences between the contours resulting from this algorithm and the contours validated by a clinical expert were analyzed. These contours were obtained following the strategy proposed by Faggiano *et al.*[14] for the case of lung structure, and manually using the MIPAV software[15] for the case of lung tumor. The differences were quantified by calculating precision indexes used in the medical field for the analysis of structures of interest[2], including the dice similarity coefficient (DICE), the mean symmetric distance between contours (DSM), and the percentage of distances greater than the voxel dimension (%DMDV)[16].

The DICE index is a measure of global precision, specifically of overlap between the structures to be compared, which can have values between 0 (absence of coincidence in the masks) and 1, which translates into a perfect overlap between the structures. These structures are represented by binary masks generated from the contours obtained in the segmentations. The calculation of the DICE index is performed as follows:

$$DICE = 2\frac{\#(A \cap B)}{\#A + \#B} \tag{13}$$

In this case, the intersection between the binary plus-faces A and B (masks to compare) is calculated, and # represents the cardinality of the sets.

The DSM is the mean value of the calculation of all Euclidean distances between the points of two contours (C_A and C_B), and is estimated as follows:

$$DSM = \frac{1}{C_A + C_B}\left(\sum_{p_A \in C_A} d(p_A, C_B) + \sum_{p_B \in C_B} d(p_B, C_A)\right) \tag{14}$$

where p_A and p_B are the voxels belonging to the contours C_A and C_B, and $d(p,C)$ is the minimum Euclidean distance between the voxels and the contour opposite to where they are located. This index provides a measure of the mean error (misalignment) present between the analyzed contours.

Finally, the %DMDDV index indicates the percentage of distances between contours that exceed an established admissible error threshold, normally the voxel dimension is used as the threshold, as this establishes a percentage of the perceptible differences between segmentations. Considering two sets defined as follows:

$$G_A = \{p_A \in C_A | d(p_A, C_B) > DimVoxel\} \tag{15}$$

$$G_B = \{p_B \in C_B | d(p_B, C_A) > DimVoxel\} \tag{16}$$

where DimVoxel refers to the voxel thickness, the %DMDDV index can be calculated as:

$$\%DMDV = \frac{\#G_A + \#G_B}{\#C_A + \#C_B} \cdot 100 \tag{17}$$

2.5 Three-dimensional reconstruction

The reconstruction of the results of both seg-

mentations (lungs and tumor) was performed through the graphing of an isosurface, using the tool already defined in the MatLab® software.

This consists of calculating the surface values of the data from a volume, which in this case are the masks resulting from the segmentations, and then connecting and adjusting these points on the *x*, *y*, and *z* axes.

In this case, each structure was reconstructed individually, and in addition, the two structures were plotted in the same plane, which allowed the two results to be observed together. To achieve this, the outer structure (lungs) had to be plotted as a transparency in order to visualize the inner tumor.

The term that gives transparency to an isosurface is *alpha*. When this term has a value closer to 0, the more translucent the reconstructed volume can be observed, while at values close to 1 the volume will take on a more opaque appearance.

The *alpha* value used for the reconstruction of the lungs was 0.1, which allowed to visualize not only the lung tumor, but also to visualize in detail the internal ramifications of the lungs.

2.6 Pulmonary dynamics

The three-dimensional reconstruction procedure was performed on the ten phases (CT images) of the respiratory cycle available in order to obtain information on the dynamics of the structures of interest throughout the respiratory cycle. In particular, for the case of the lung tumor, we sought to calculate the maximum displacements (in millimeters) in each cartesian axis.

This is possible to obtain using the reconstructions of the lung tumor in the phases of the beginning of inspiration and the beginning of expiration, together with the information of the voxel dimension (0.98 mm × 0.98 mm × 2.00 mm). This information is important because it could be used in the planning of tomotherapy treatments.

3. Results and discussion

3.1 Iteration definition analysis

To determine the number of iterations for the lung and lung tumor segmentations, a robustness and consistency analysis of the proposed algorithm was performed, in which the result of a segmentation using a maximum number of 100 iterations was compared with the result of segmentations using iterations of 5, 10, 20, ..., up to 100. Taking into account the above, **Figure 2** shows the difference in voxels between the result of the segmentation of the lungs with 100 iterations compared to the result of the other segmentations (from 5 to 100). Additionally, in this figure, a red line can be observed at the value of 600 voxels, which represents that there is a difference of 0.01%. Thus, it is possible to appreciate that the segmentations are very similar (consistent) regardless of the number of iterations used in a range between 5 and 100 iterations; however, the number of iterations was set to that value that had an error below 0.01%, which corresponds to a number of 10 iterations for the case of lung segmentation. For the lung tumor segmentation, the same procedure was performed in order to determine that the minimum number of iterations necessary for a consistent segmentation was set at 5.

It is important to mention that although it seems that the number of iterations does not seem to have a great impact on the accuracy of the segmentation, the minimum number of iterations is sought in order to obtain a good result in the shortest possible time. Therefore, for the case of the three-dimensional segmentation of the lungs with 10 iterations, the computation time was approximately 10 minutes, while for the lung tumor the segmentation took 4 minutes with 5 iterations. In all cases the segmentations were performed on a mid-range laptop computer (Intel Core i7 @2.5 *GHz* processor with 8 *GB* of RAM).

3.2 Evaluation and quantitative analysis of 3D segmentations

For the visual presentation of the results obtained by the proposed method, the CT image in the final phase of expiration was used, which was considered in this work as the reference image. **Figure 3** shows a central slice of the CT image of the image, showing the original image (**Figure 3a**) and the results of the segmentation of the structures using the proposed method; lungs (**Figure 3b**) and lung tumor (**Figure 3c**).

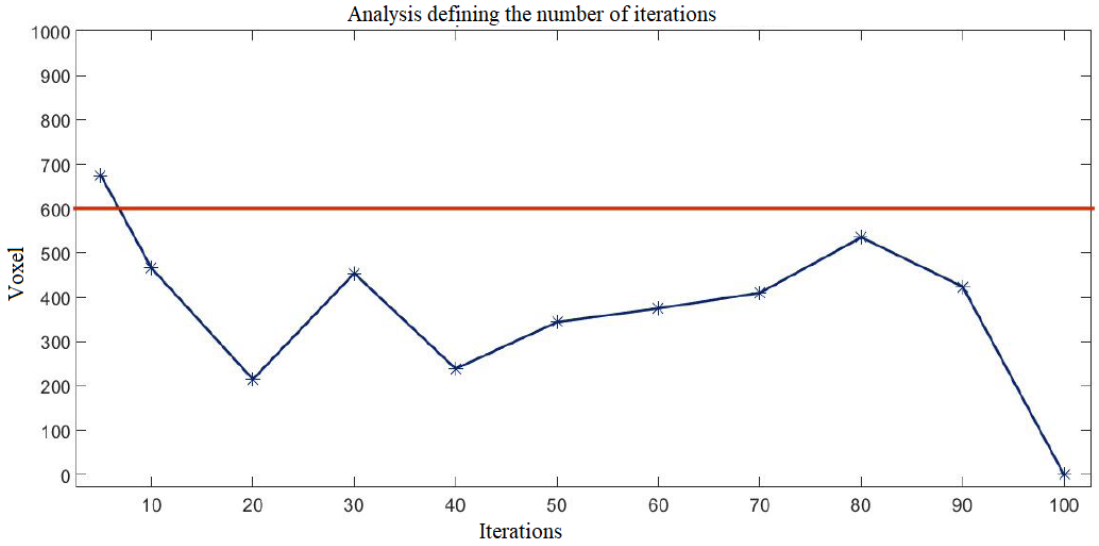

Figure 2. Difference in voxels between segmentations using different number of iterations.

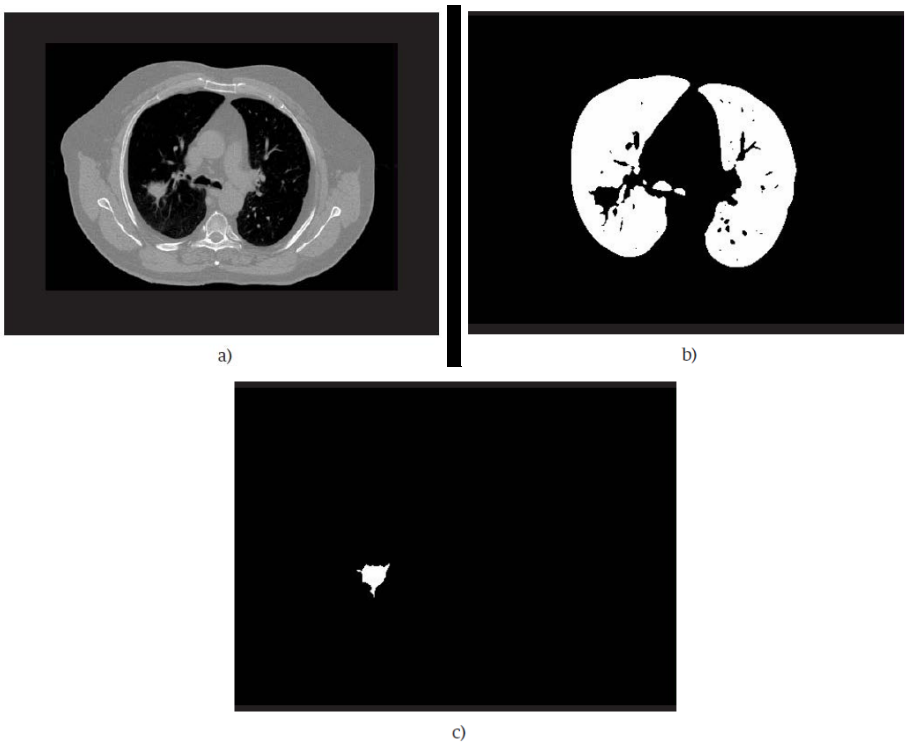

Figure 3. Segmentation results of the structures of interest. (**a**) CT image of lung and tumor (reference phase); (**b**) lung contour obtained by the proposed method; (**c**) lung tumor contour obtained by the proposed method.

In **Figure 3** it is possible to appreciate that the implemented method performs a good segmentation of both anatomical structures of interest, since it manages to efficiently define their contours. In the case of the lungs, the method manages to define the external border of the lungs, and also manages to segment their internal characteristics (bronchial ramifications), which are visible in **Figure 3a**. As for the lung tumor, the proposed algorithm manages to adequately segment the complex shape of this anatomical structure, being able to differentiate small details located in the periphery of the tumor. This reinforces the conclusions reported by Hernandez *et al.*[8], i.e., that the Chan-Vese method is robust and accurate for the segmentation of anatomical structures of different sizes and shapes.

To reinforce the results of the good qualitative performance shown in **Figure 3**, **Table 1** shows the results from the calculation of the precision indexes as a quantitative complement to the evaluation of

the segmentations obtained by the proposed method.

In **Table 1**, the good performance of the implemented method in the segmentation of the lung and tumor structures can be verified. For the DICE index, values close to 1 were found (above 0.90 for the case of the lungs and above 0.80 for the case of the tumor), which shows a great similarity of the result obtained with the contours validated by the clinical expert, regardless of the dimension and shape of the structures.

As for the *DSM* index, it has a mean error value of 2.55 mm for the case of the lungs, which may be due to the details (internal ramifications) that the proposed method is able to segment and that in the reference segmentation are not considered by the clinical expert. This suggests that the more details found inside the lungs, the higher the *DSM* value and therefore also the %DMDV value, which reflects the percentage of distances greater than a set threshold, which in this case corresponds to 2 mm (voxel thickness).

Table 1. Accuracy index results for the quantitative analysis of the segmentations of the structures of interest

Indice	Structures of interest	Lungs tumor
DICE	0.94	0.82
DSM (mm)	2.55	0.41
%DMDV (%)	29.25	0.01

However, for the case of the tumor, these two indices show values very close to 0, which speaks of a great similarity of the expert's manual contours with the segmentation resulting from the proposed method, to such a degree that the differences are smaller than the voxel dimension.

3.3 Three-dimensional reconstruction

Figure 4 shows the three-dimensional reconstructions of the results of the segmentations in the reference phase, where the structure of the lungs (**Figure 4a**) and the lung tumor (**Figure 4b**) can be better observed. Additionally, the representation of both three-dimensional structures in the same plane is shown (**Figure 4c**), where it is possible to identify the tumor in red and the lungs as a transparency, which allows us to observe their internal ramifications.

These reconstructions allow us to know in detail the characteristics of the structures of interest, such as their shape and size, and in the case of lung tumor, it also allows us to visualize and confirm its location within the lungs by means of transparency.

3.4 Pulmonary dynamics

Finally, **Figure 5** shows the reconstructions of both anatomical structures of interest in the ten phases of the respiratory cycle, where we can observe the inspiratory phase (**Figure 5a**–**e**), being **Figure 5a** the beginning of inspiration, and the expiratory phase (**Figure 5f**–**j**)), which begins in **Figure 5f**.

Figure 5 allows us to appreciate the displacement generated both in the lungs and in the tumor due to respiration. To improve the detail in the dynamics of the tumor, we added some guides (blue lines) that allow us to check the maximum displacement of the tumor on the *z*-axis of 17 transverse slices, corresponding to 34.0 *mm* (using the information of the voxel dimension), between the phases of the beginning of inspiration and the beginning of expiration. With respect to the *x*-axis and *y*-axis, the tumor had a smaller displacement of 2.9 mm and 3.9 mm, respectively.

It is important to mention that the maximum displacement along the *z-axis* was expected, since anatomically the movement generated by the diaphragm along this axis is much greater than the displacement of the thoracic walls due to inspiration and expiration. These results confirm the influence of breathing on the movement of the anatomical structures studied, and the maximum displacements obtained could be used in the planning of tomotherapy treatments.

4. Conclusions

In this work we presented the implementation of an active contour segmentation method based on the Chan-Vese algorithm to extract anatomical structures of interest in 4DCT images of the chest. The proposed algorithm succeeds in properly segmenting both lungs and the lung tumor present in the images, confirming that the method is capable of segmenting structures of different sizes and

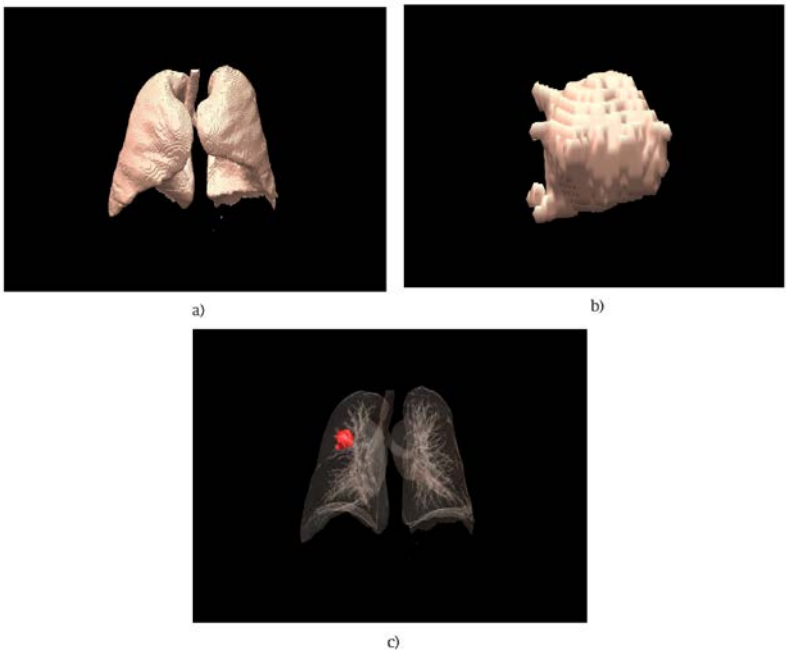

Figure 4. Three-dimensional reconstruction of the structures of interest. (**a**) Reconstruction of the lungs; (**b**) 3D reconstruction of the lung tumor; (**c**) reconstruction of the lung and tumor structures in the same plane.

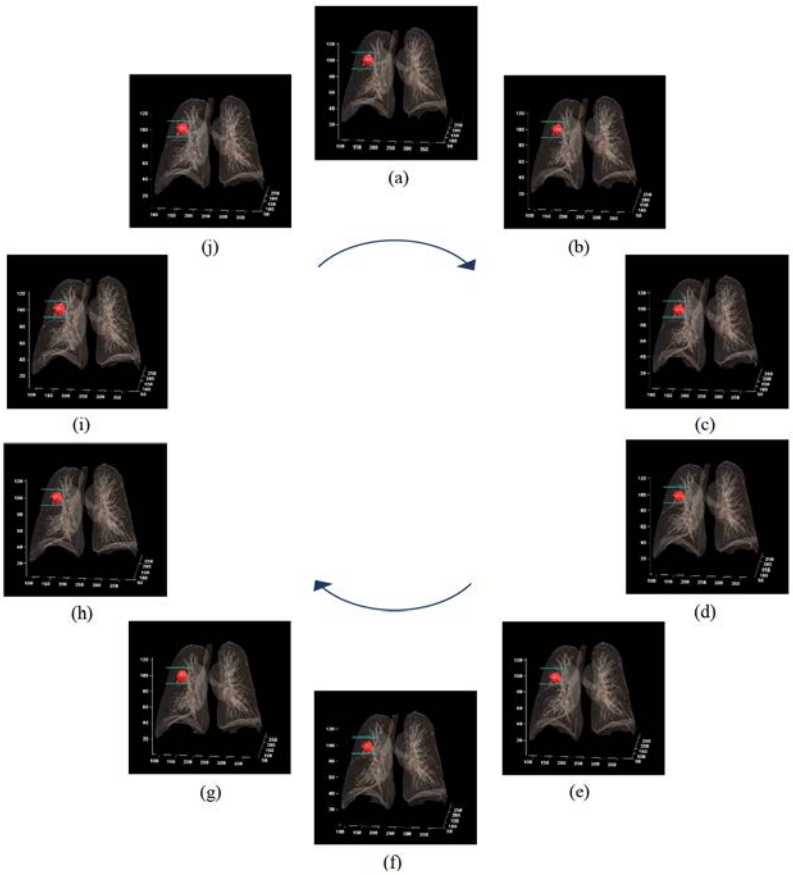

Figure 5. Three-dimensional reconstruction of lung structures and lung tumor in the phases of the respiratory cycle. (**a**–**e**) Inspiratory phase; (**f**–**j**) expiratory phase. The *x*, *y* axes are pixels and the *z* axis are cross sections.

shapes. Specific characteristics of each anatomical structure can be known in detail by means of the three-dimensional reconstruction, in addition to the location of the structures of interest (tumor), infor-

mation that can be of great importance in radiotherapy and tomotherapy treatments, where the aim is to minimize radiation in healthy organs near the cancer cells.

It is important to mention that the results presented in this work correspond only to a set of 4DCT images of a study subject, therefore, it is expected in the future to be able to perform the same procedure to a database with more patients. Additionally, comparisons will be made between the proposed algorithm and other segmentation and reconstruction methods in the state of the art RT applications, so that more evidence of the good performance of the proposed algorithm can be obtained. Finally, it is expected to have feedback from medical physicists to validate the possible use of the information of the maximum displacements obtained in the planning of tomotherapy treatments.

Conflict of interest

The authors declared no conflict of interest.

References

1. Aubert G, Kornprobst P. Mathematical problems in image processing: Partial differential equations and the calculus of variations. Springer Science and Business Media 2006; 147. doi: 10.1007/978-0-387-44588-5.
2. Faggiano E, Fiorino C, Scalco E, *et al*. An automatic contour propagation method to follow parotid glands deformation during head-and-neck cancer Tomotherapy. Physics in Medicine and Biology 2011; 56(3): 775–791. doi: 10.1088/0031-9155/56/3/015.
3. Fox J, Ford E, Redmond K, *et al*. Quantification of tumor volume changes during radiotherapy for non-small-cell lung cancer. International Journal of Radiation Oncology Biology Physics 2009; 74(2): 341–348. doi: 10.1016/j.ijrobp.2008.07.063.
4. Mageras GS, Mechalakos J. Planning in the IGRT context: Closing the loop. Seminars in Radiation Oncology 2007; 17: 268–277. doi: 10.1016/j.semradonc.2007.06.002.
5. Pal NR, Pal SK. A review on image segmentation techniques. Pattern Recognition 1993; 26(9): 1277–1294. doi: 10.1016/0031-3203(93)90135-J.
6. Chandhok C, Chaturvedi S, Khurshid AA. An approach to image segmentation using K-means clustering algorithm. International Journal of Information Technology 2012; 1: 11–17.
7. Otsu N. A threshold selection method from gray-level histograms. IEEE Transactions on Systems, Man, and Cybernetics 1979l; 9(1): 62–66. doi: 10.1109/TSMC.1979.4310076.
8. Hernandez S, Mejia AR, Arce ER, *et al*. Evaluación cuantitativa del desempeño de métodos de segmentación aplicados a imágenes médicas para el análisis de estructuras anatómicas de interés (Spanish) [Quantitative evaluation of the performance of segmentation methods applied to medical images for the analysis of anatomical structures of interest]. Memorias Congreso Nacional de Ingeniería Biomédica 2015; 2: 374–377.
9. Vandemeulebroucke J, Rit S, Kybic J, *et al*. Spatiotemporal motion estimation for respiratory-correlated imaging of the lungs. Medical Physics 2011; 38(1): 166–178. doi: 10.1118/1.3523619.
10. Jianyuan D, Chongyang H. 3D fast level set image segmentation based on Chan Vese model. 3rd International Conference on Bioinformatics and Biomedical Engineering; 2009. p. 11–13. doi: 10.1109/ICBBE.2009.5162136.
11. Liu L, Zeng L, Luan X. 3D robust Chan-Vese model for industrial computed tomography volume data segmentation. Optics and Lasers in Engineering 2013; 51(11): 1235–1244. doi: 10.1016/j.optlaseng.2013.04.019.
12. He F, Sun Y. Segmentation of noisy CT volume data using improved 3D Chan-Vese model. 2015 IEEE 7th International Conference on Awareness Science and Technology (iCAST); 2015. p. 31–36. doi: 10.1109/ICAwST.2015.7314016.
13. Chan TF, Vese LA. Active contours without edges. IEEE Transactions on Image Processing 2001; 10(2): 266–277. doi: 10.1109/83.902291.
14. Faggiano E, Cattaneo GM, Ciavarro C, *et al*. Validation of an elastic registration technique to estimate anatomical lung modification in non-small-cell lung cancer tomotherapy. Radiation Oncology 2011; 6(1). doi: 10.1186/1748-717X-6-31.
15. McAuliffe MJ, Lalonde FM, McGarry D, *et al*. Medical image processing, analysis and visualization in clinical research. Proceedings of the 14th IEEE Symposium on Computer-Based Medical Systems. Washington: IEEE Computer Society. 2001. p. 381. doi: 10.1109/CBMS.2001.941749.
16. Mejia AR. Deformable image registration for radiotherapy monomodal applications [PhD thesis]. Milan: Politecnico di Milano; 2013. Available from: https://www.politesi.polimi.it/handle/10589/82803.